J. Fluid Mech. (1982), *vol.* 116, *pp.* 297–313
Printed in Great Britain

Droplet drag in an accelerating and decelerating flow

By S. TEMKIN AND H. K. MEHTA†
Department of Mechanical and Aerospace Engineering, Rutgers University, New Brunswick, New Jersey 08903, U.S.A.

(Received 11 August 1980 and in revised form 31 July 1981)

An experimental study of the motion of small water droplets in both accelerating and decelerating conditions is presented. Droplets with diameters in the range 115–187 μm were exposed to propagating N-waves having strengths smaller than 0·03. Droplet-displacement data were obtained by single-frame stroboscopic photography, at an equivalent framing rate of 4000 pictures per second. The data were fitted by means of best-fit polynomials in time, which were used to obtain drag coefficients in accelerating and decelerating flow conditions. In addition to providing drag data for impulsive-type motions, these data show that the unsteady drag follows two entirely distinct trends. In one, applicable to decelerating relative flows, the unsteady drag is always larger than the steady drag at the same Reynolds number. In the other, applicable to accelerating relative flows, the unsteady drag is always smaller than the corresponding steady value. These trends have not been previously known. They give some support to a mechanism recently proposed (see Temkin & Kim 1980) to explain departures of the drag coefficient for a sphere from its steady value; namely, the changes in size of the recirculating region behind the sphere, relative to its steady counterpart at the same Reynolds number.

1. Introduction

The drag coefficient for small droplets moving in air is of some importance in many scientific and technological applications. For steady conditions, experimental results exist which show that, for non-deforming droplets, it is nearly equal to that for steadily moving rigid spheres. However, the only situations where small spheres are known to move steadily occur when they achieve terminal velocity in a stagnant fluid, and when they are fully carried by a steadily moving fluid. Neither situation is representative. In actual conditions, the motion of a droplet relative to the supporting fluid is always unsteady, and the question remains as to what are the forces that act on the droplet.

The problem of unsteady motions of small particles has received considerable attention. Several critical reviews of the literature have been recently presented by Torobin & Gauvin (1959), by Hill (1973) and by Clift, Grace & Weber (1978). The experimental studies include works on spheres released from rest in a quiescent fluid (Lunnon 1926), works on spheres moving according to prescribed time dependences (Odar & Hamilton 1964; Roos & Willmarth, 1971; Karanfilian & Kotas 1978), and works on spheres moving in response to a moving fluid (Ingebo 1956; Selberg & Nicholls 1968; Hill 1973; Reichman 1973; Rudinger 1974; Kim 1977). Although the

† Present address: Boeing Commercial Airplane Co., Seattle, Washington, U.S.A.

motions considered in these studies are not the same, and the Reynolds-number ranges covered do not coincide, the general conclusion that emerges from them is that the actual drag on the spheres differs from the steady drag. However, there seems to be no agreement on the mechanism responsible for the departures.

Recently, Temkin & Kim (1980) reported some experimental results that show that the drag coefficient acting on non-deforming droplets accelerating in the uniform flow behind a weak shock wave is larger than the steady drag at the same Reynolds number. The differences were ascribed to changes in the recirculating region behind the droplet, brought about by the unsteadiness of the relative fluid velocity. In particular, it was argued that, when this velocity decreases in time, the size of the recirculating region is larger than for steady flow at the same Reynolds number, thereby producing a larger drag. To test this proposed mechanism, they correlated their drag data with the non-dimensional relative-acceleration parameter

$$A = \left(\frac{\rho_p}{\rho_0} - 1\right) \frac{D}{U_r^2} \frac{dU_r}{dt}, \tag{1}$$

where D is the droplet diameter, and U_r is the magnitude of the relative velocity between fluid and droplet, and found that the experimental results could be expressed as

$$C_D = C_{DS} - K\left(\frac{\rho_p}{\rho_0} - 1\right) \frac{D}{U_r^2} \frac{dU_r}{dt}, \quad \frac{dU_r}{dt} < 0, \tag{2}$$

where C_{DS} is the steady drag coefficient, and K is a constant of order 1.†

These results are strong evidence that unsteadiness produces departures of the drag from its unsteady value. However, since, in the experiments of Temkin & Kim, the droplets accelerated in the uniform-velocity region behind a normal shock wave, dU_r/dt was always negative. It was, therefore, not possible to measure drag coefficients under the condition $dU_r/dt > 0$. Further, data for the case $dU_r/dt > 0$ are also needed to test the mechanism proposed to explain the measured departures. This mechanism implies that, if $dU_r/dt > 0$, the recirculating region behind the sphere should be smaller than for steady flow, thereby producing a smaller drag than the steady flow at the same Reynolds number.

In this work, we present drag coefficients for small droplets undergoing both positive and negative accelerations. This type of motion is accomplished by exposing the droplets to N-waves. In these, the fluid velocity decreases from some value immediately behind the leading shock, to a value of similar magnitude, but having the opposite direction, immediately ahead of the trailing shock. Thus, owing to the passage of the wave, a droplet will first experience large positive accelerations which

† The algebraic dependence on the density ratio displayed by (1) is not implied. The dimensional arguments given by Temkin & Kim show that, for a rigid sphere moving unsteadily in a fluid, the drag coefficient may be expressed as

$$C_D = C_D\left[R, g(\rho_p/\rho_0) \frac{D}{U_r^2} \frac{dU_r}{dt}\right],$$

where $g(\rho_p/\rho_0)$ is some function of the density ratio. For convenience, the function shown in (1) was selected. This choice has no effect on the data or on the fit, because the density ratio was constant. Thus, variations of A only represent variations of the non-dimensional acceleration $(D/U_r^2)\,(dU_r/dt)$.

impart to the droplet a velocity in the direction of the flow, producing initially a decrease of the relative fluid velocity. However, owing to the deceleration of the fluid velocity in the wave, the relative velocity will eventually increase in time.

Our experiments were conducted with water droplets having diameters in the range of 115–187 μm. The maximum flow velocity to which the droplets were exposed was 1010 cm/s, giving a maximum Weber number equal to 0·137, a value well below that for which deformation is noticeable (Temkin & Kim 1980). Our drag data show two distinct trends. In particular, in the Reynolds number range $9 < R < 115$, where the estimated errors in the Reynolds number are smaller than 15 %, best fits for our data give

$$C_D = C_{DS} - k_1 A \quad (-45 < A < -3), \tag{3}$$

$$C_D = C_{DS} - k_2 A^{-1} - k_3 \quad (5{\cdot}9 < A < 25), \tag{4}$$

where $k_1 = 0{\cdot}048$, $k_2 = 3{\cdot}829$ and $k_3 = 0{\cdot}204$.

In the transition region, the experimental accuracy is not sufficiently good to elucidate the behaviour of the positive-A branch, as $A \to 0$. This behaviour remains a most important unknown in the study of the effects of unsteadiness on droplet drag.

2. Experimental apparatus and procedure

The main components of the experimental apparatus used in this investigation include a conical-driver shock tube, a droplet generator, and a high-speed photographic system. These components are briefly described below. A more detailed description is given elsewhere (Mehta 1980).

2.1. *Conical-driver shock tube*

Several techniques exist that can be used to produce N-waves. The one we selected is based on the so-called spherical-balloon problem. Here, a pressurized, spherical region is allowed to expand suddenly. As is well known (see e.g. Lamb 1925), the expansion produces an N-wave. By analogy, a long cone with a pressurized region near the vertex can also be used to produce such waves at some distance from that region. However, because of practical considerations, we adopted a design in which only the high-pressure portion is conical, and the driven portion has a constant cross-sectional area. To minimize disturbances produced by the sudden variation of the rate of change of the cross-sectional area, we selected a cone having an internal angle of only 5°, and a length of 116 cm. Because of its dimensions, the cone had to be made of six smoothly joining sections. The constant-cross-section portion of the facility is 369 cm long and has a 10·2 cm inside diameter. The facility and its related instrumentation are shown schematically in figure 1.

Figure 2 shows a typical pressure-amplitude-versus-time record obtained with the above-described facility. The exact time interval between the forward and trailing shocks, i.e. the 'test time', changes with amplitude owing to nonlinear effects, but for the small amplitudes used in our tests it was nearly constant and equal to 6·8 ms. This time closely corresponds to the acoustic limit $t_s = 2x_0/c_0$, where x_0 is the length of the pressurized cone, and c_0 is the speed of sound in the low-pressure region.

In our experiments we require the fluid velocity between the two shocks. To obtain

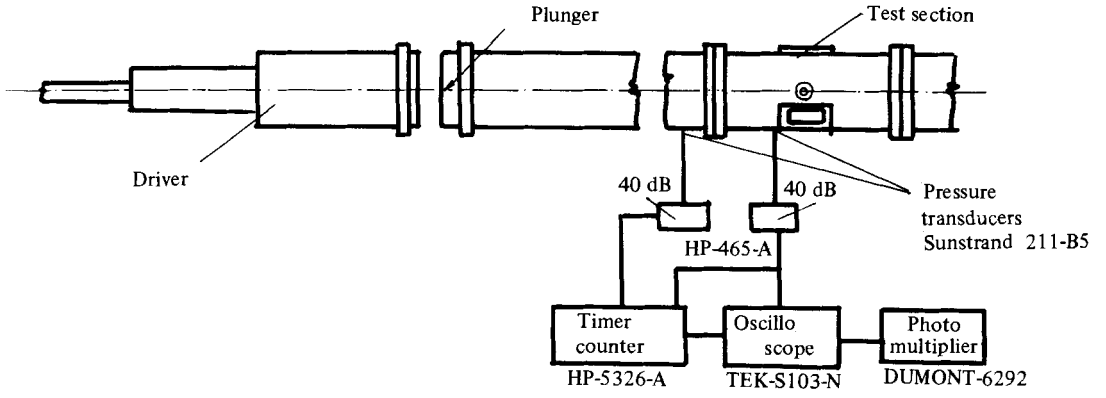

FIGURE 1. Conical-driver shock-tube facility.

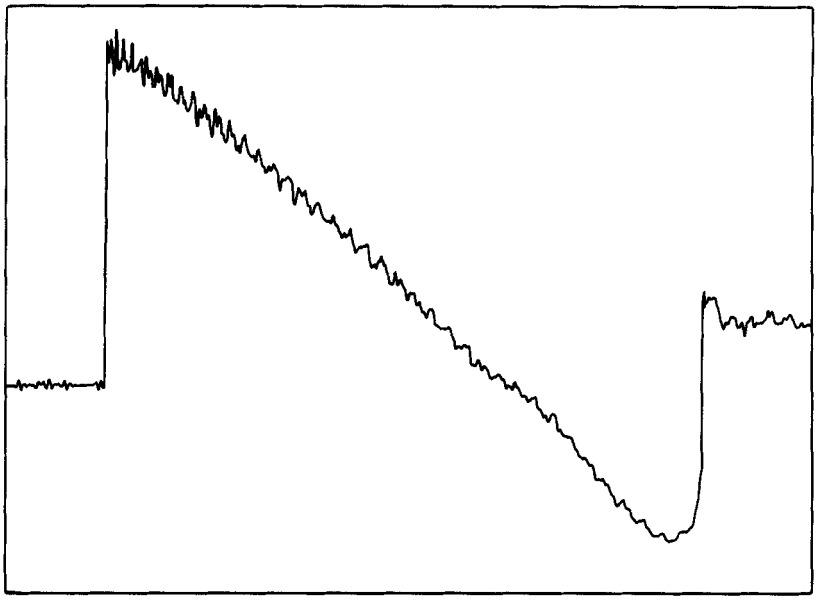

FIGURE 2. Typical pressure-versus-time profile.

this quantity, we make use of the fact that, as shown by shadowgraphs, the leading shock is a normal shock. Thus, the fluid properties on both sides of it are connected by the usual normal-shock relations, i.e.

$$u_{t_1} = \frac{\frac{c_0}{\gamma}\left(\frac{p_1}{p_0} - 1\right)}{\left[1 + \frac{\gamma+1}{2\gamma}\left(\frac{p_1}{p_0} - 1\right)\right]^{\frac{1}{2}}}, \tag{5}$$

$$T_1 = T_0 \frac{p_1}{p_0}\left(1 + \frac{\gamma-1}{2\gamma}\frac{p_1}{p_0}\right)\left(\frac{p_1}{p_0} + \frac{\gamma-1}{2\gamma}\right)^{-1}, \tag{6}$$

$$c_1 = c_0(T_1/T_0)^{\frac{1}{2}}, \tag{7}$$

D (cm)	f (Hz)	λ/D
0·0115	3400	8·8
0·0135	2500	8·0
0·0152	2400	9·9
0·0167	920	13·6
0·0183	1000	14·4

TABLE 1. Droplet-stream characteristics

where the subscript 0 refers to the properties in the undisturbed region ahead of the shock, and the subscript 1 refers to properties on the other side of the shock. Thus, the quantity u_{f_1} is the maximum fluid velocity, $U_{\max}$ in the wave. The flow velocity in the remaining portion of the wave may then be obtained by treating it as a simple wave. Thus,

$$u_f = u_{f_1} + \frac{2c_1}{\gamma - 1}\left[\left(\frac{p}{p_1}\right)^{(\gamma-1)/2\gamma} - 1\right], \tag{8}$$

$$c = c_1 + \tfrac{1}{2}(\gamma - 1)(u_f - u_{f_1}), \tag{9}$$

$$T = (c/c_1)^2 T_1. \tag{10}$$

These equations give the fluid velocity near the centre of the tube (i.e. far from wall-induced effects), on a cross-sectional plane that intersects the tube at the location of the pressure transducer. On the other hand, what is required for computing the drag is the fluid velocity at the instantaneous location of the droplets, and these are injected downstream of the transducer. However, since the instantaneous locations of the droplets are known, the required fluid velocity can always be calculated.

2.2. *Droplet generator*

The droplets used in our experiments were produced by the well-known capillary instability of a liquid jet. The generator we used was described earlier by Temkin & Kim. The main characteristics of the droplet streams we used are shown in table 1. Two significant differences between these streams and those used earlier should be pointed out. First, in order to attain small Reynolds numbers, they used droplets as small as 85 μm in diameter. In our case, because of the reversal of the relative fluid velocity, such small droplets were not necessary. Second, our interdroplet separation is about 3 times larger than theirs. This advantageous increase was achieved by the use of lower frequencies and slightly larger pinhole diameters.

2.3. *Droplet photography*

The droplet streams produced in the manner described above are allowed to fall through the horizontal test section of the tube. Before the passage of the wave, the droplets' motion is along the vertical. Afterwards, they acquire a horizontal component which is parallel to the tube axis. Thus the droplet motion takes place in a plane, making it possible to obtain time-resolved photographic records of droplet trajectories. These were obtained by recording on a single negative the stroboscopic light scattered

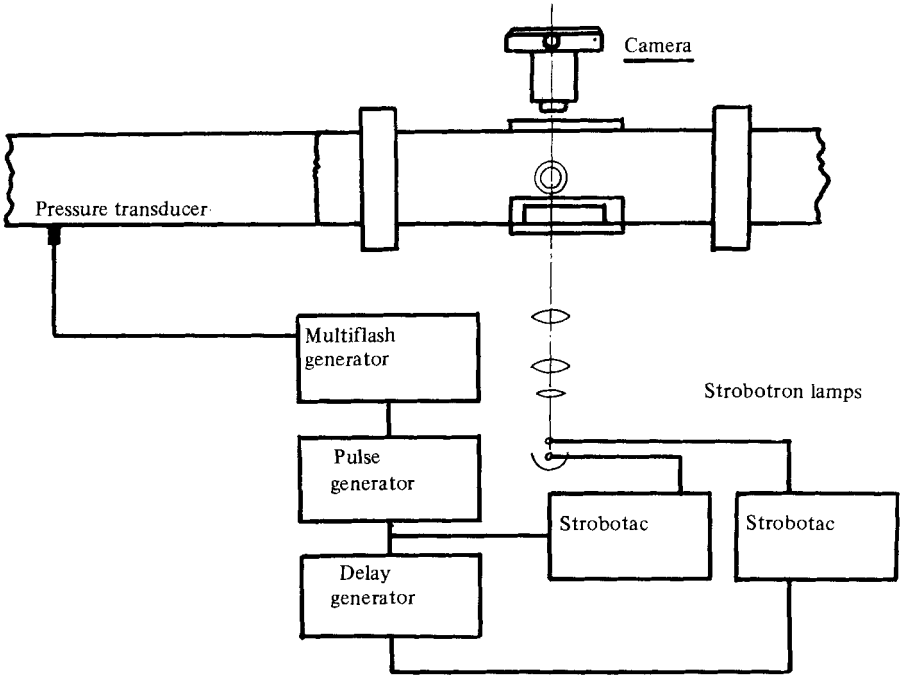

FIGURE 3. Electronic system for flash control.

by the droplets. Our procedure differs from that used earlier in that the incident-light-beam arrangement contained two stroboscopic lamps, rather than one, thus doubling the flashing rate. The combination provided an equivalent framing rate of up to $5000\,s^{-1}$.

The electronic system that was used to obtain such high flashing rates is shown schematically in figure 3. A signal from one of the pressure transducers (Sunstrand Model 211-B5), is delayed by a multiflash generator (General Radio Model 1541) which triggers a pulse generator (Hewlett Packard Model 8011A). This produces a predetermined number of pulses. Because of the limitations of the stroboscopic lamps used in this investigation (General Radio Model 1538), the minimum interval between pulses was $400\,\mu s$ (corresponding to a flashing rate of $2500\,s^{-1}$). Each of these pulses produces a flash in the first stroboscope. Nearly simultaneously with the flash, the first stroboscope gives an output pulse. This, in turn, is delayed by a delay generator (Berkley Nucleonics Model 7010). After the delay, the pulse is fed into a second stroboscope where it produces a second flash. To ensure proper flashing, the pulse separation and the time delay we used were 500 and $250\,\mu s$, respectively, giving a flashing rate of $4000\,s^{-1}$. As in our earlier work, a photomultiplier was used to monitor the flashing sequence and to count the actual number of flashes during a test. Typically, this number was 25 or larger. Thus, the number of displacement-data points during a given test was at least 25. While this number may appear to be small, it represents a fivefold increase over the number of data points per test used in similar experiments elsewhere. Furthermore, our data is collected on a single negative, thus eliminating the errors that would exist had the data been obtained from several negatives, as is the case when high-speed framing cameras are used.

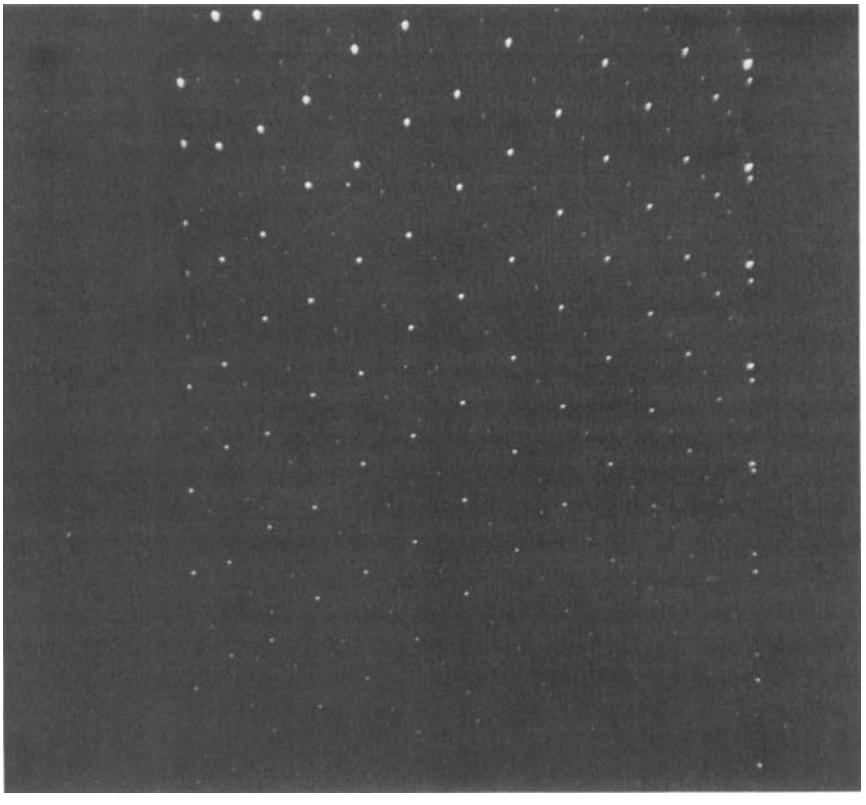

FIGURE 4. Typical reflected-light photograph of droplets during one test. Flow is from right to left.

Figure 4 shows a typical photograph obtained in the above manner. It shows the light scattered by a droplet stream at several instants after the passage of the wave front. It should be noticed that every droplet in the droplet stream moves equal distances between flashes. This is important, for it shows that the flow is one-dimensional. It can also be seen in figure 4 that there are differences in the brightnesses of the light scattered by consecutive droplet streams. The differences occur because the second stroboscope lamp had to be placed slightly off its optimum location in the optical arrangement.

3. Data analysis and results

Photographs of the type shown in figure 4 were used to determine droplet trajectories. The procedures used to do this were identical with those used earlier by Temkin & Kim, and will not be repeated here. Figure 5 shows trajectories of droplets having the same diameter, responding to N-waves having different maximum velocities. Figure 6 shows trajectories of different-sized droplets responding to N-waves having the same strength. The horizontal-displacement data corresponding to figures 5 and 6 are shown in figures 7 and 8. A total of 17 different trajectories having a maximum Weber number smaller than 0·15 were obtained. As explained in our earlier work, no deformation of the droplet's surface could be observed below this number. The corresponding

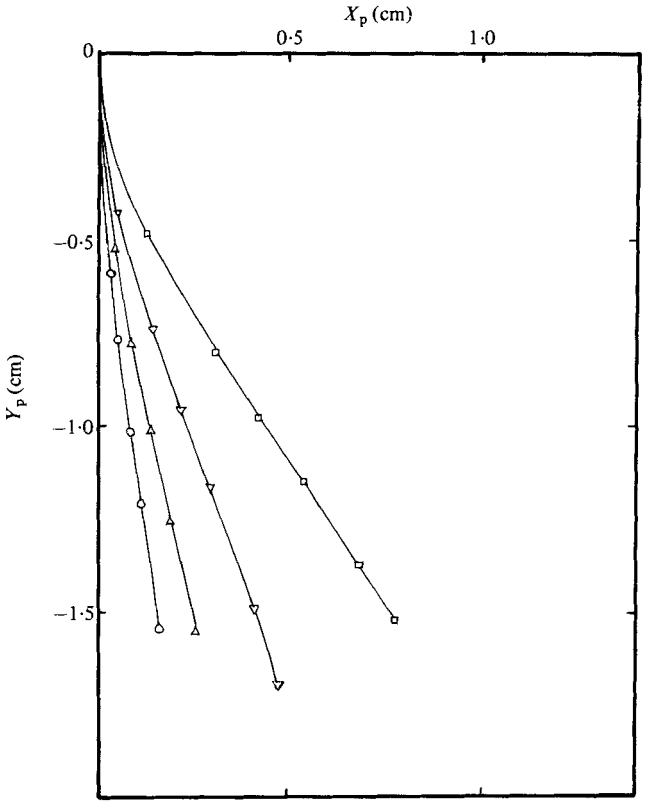

FIGURE 5. Trajectories of 135 μm droplets. ○, U_{max} = 305·6 cm/s; △, 403·7 cm/s; ▽, 704·3 cm/s; □, 985·6 cm/s.

displacement data were fitted by means of best-fit polynomials, of the form

$$X_p = a_0 + a_1 t + a_2 t^2 + a_3 t^3, \tag{11}$$

$$Y_p = b_0 + b_1 t + b_2 t^2 + b_3 t^3. \tag{12}$$

The degree of the polynomials was selected from analysis of the standard errors associated with polynomials of degrees 1–6. In all cases the standard deviation for the displacement polynomials was less than 3 μm.

The polynomials were used to compute droplet velocities and accelerations. Figure 9 shows the horizontal displacement, velocity and acceleration in one of our tests. It may be noted that the initial acceleration is rather large, and that it decreases in time, eventually changing sign, a result of the droplet velocity becoming larger than that of the fluid.

To obtain the drag coefficient from our experimental data, we make use of

$$C_D = \tfrac{4}{3} D \frac{\rho_p}{\rho_0} \frac{(du_p/dt)^2}{(u_f - u_p)^2 [(du_p/dt)^2 + ((dv_p/dt) + g)^2]^{\frac{1}{2}}}. \tag{13}$$

Here, u_f and u_p are the horizontal velocity components of the fluid and of the droplet, respectively, v_p is the vertical velocity of the droplet, and g is the acceleration due to gravity. By fluid velocity we mean the velocity that the fluid would have at the droplet location in the absence of the droplet. Also needed is the Reynolds number.

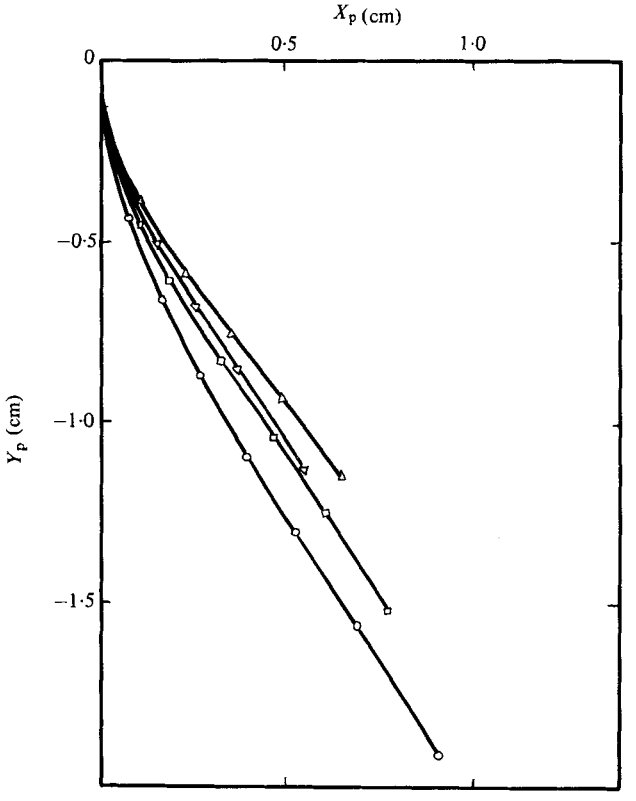

FIGURE 6. Trajectories of different-sized droplets in N-waves having nearly equal maximum velocities, $U_{max} \simeq 990$ cm/s. ○, $D = 120\,\mu$m; □, 135 μm; △, 167 μm; ▽, 183 μm.

This is given by

$$R = \frac{\rho_0 |\bar{U}_f - \bar{U}_p| D}{\mu}, \tag{14}$$

where

$$|\bar{U}_f - \bar{U}_p| = U_r = (u_f - u_p) \frac{[(du_p/dt)^2 + ((dv_p/dt) + g)^2]^{\frac{1}{2}}}{du_p/dt}, \tag{15}$$

is the magnitude of the relative velocity. Equations (13) and (15) apply only to two-dimensional motions (see Temkin & Kim 1980, §2).

4. Results

Figure 10 shows drag coefficients obtained in one of our tests. As customary, we show C_D as a function of the Reynolds number R. The data points are numbered sequentially from $t = 0$. The numbers have a one-to-one correspondence with the sequential numbering of the flashes. The numerical data from which figure 10 was prepared is shown in table 2. Also shown in the figure are the estimated confidence bars for the Reynolds number. The corresponding estimated errors for the drag coefficients are larger than those for the Reynolds number, as indicated in table 2. The confidence bars include the errors associated with the higher-order derivatives of the displacement polynomials, as well as errors in the measurements of pressure and in the

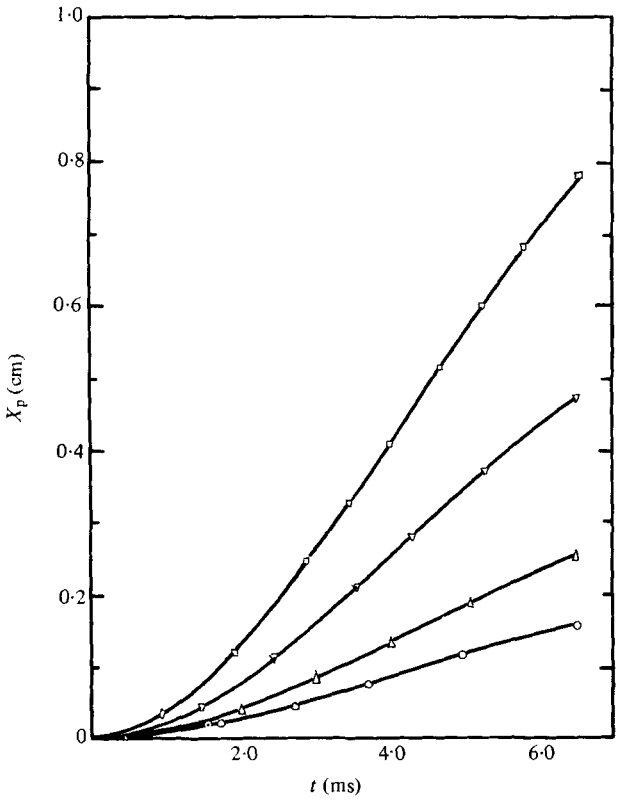

FIGURE 7. Horizontal displacement of 135 μm droplets in several tests. □, U_{max} = 305·6 cm/s; △, 403·7 cm/s; ▽, 704·3 cm/s; □, 985·6 cm/s.

computation of the fluid velocity. Such estimates are often omitted in work of this type as they require a large number of closely spaced data points. As pointed out earlier, we had at least 25 data points per trajectory, and this number was sufficient for an accurate assessment of the errors. These errors ranged from few per cent to very large values (for details see Mehta 1980). As in our previous work, we eliminate from consideration data points having an estimated Reynolds-number error larger than 15 %. This step eliminates those data points denoted by filled symbols in figure 10. These points occur near the time when the horizontal relative velocity reverses direction. At such times, both $u_f - u_p$ and du_p/dt are very small, so that, as (13) and (15) show, the errors associated with the first and second derivatives of the displacement polynomials produce very large errors in both C_D and R.

Figure 11 shows all of our data having estimated errors in the Reynolds number smaller than 15 %. Also shown in the figure is the steady-drag coefficient. As with measurements reported earlier, the data clearly show that the drag on spheres moving unsteadily differs substantially from the steady drag. Further, the data show two distinct trends. The first, denoted by open symbols, have drag coefficients larger than the steady, and are associated with negative values of the relative-acceleration parameter A. The second, denoted by filled symbols, have drag coefficients smaller than the steady, and are associated with positive values of A.

The drag data as displayed in figure 11 obscure the fact that they were obtained

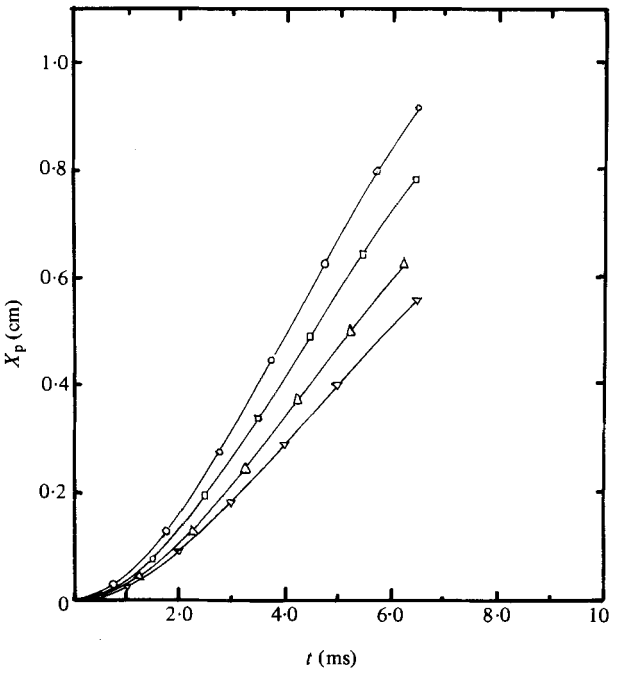

FIGURE 8. Horizontal displacement of different-sized droplets responding to equal-strength N-waves. ○, D = 120 μm; □, 135 μm; △, 167 μm; ▽, 183 μm.

under unsteady conditions. To display the dependence on unsteadiness, we consider data having approximately equal Reynolds numbers, but different values of A. As in our earlier work, a small number of such data were found. Figure 12 shows the variation of C_D versus A for the three Reynolds numbers for which both positive and negative values of A were found. The points with $A = 0$ refer to the steady case, and were taken from the steady-drag curve. The trends for $A < 0$ are similar to those found in our earlier work (see figure 20 of Temkin & Kim 1980); that is, they show that C_D increases with $-A$, and that the rate of increase seems to be independent of the Reynolds number. For $A > 0$, all the drag data available have values smaller than the steady drag, and seem to approach their corresponding steady values as A increases at a rate which appears to be independent of the Reynolds number. These statements are illustrated in figure 13, which shows, for the data of figure 12, the difference $C_D - C_{DS}$ as a function of A. While there is some scatter, and while the number of data available is not very large, figure 13 shows clearly that $C_D - C_{DS}$ depends only on A.

The same trends hold for all the data as shown in figure 14. The solid lines passing through the data points are least-square fits, and are given by (3) and (4). The results for $A < 0$ are similar to those obtained by Temkin & Kim, except that the magnitude of the coefficient K is considerably smaller in the present case. Because of the nature of the two unsteady flows, such differences were to be expected. Thus, in the earlier work, the droplets were exposed to transient flows having a constant velocity profile, so that they experienced large absolute accelerations during the entire duration of the test. In the present case, however, the droplets are exposed to transient flows having a velocity that decreases in time. Therefore, the large acceleration initially imparted to them decreases rapidly in time (see figure 9).

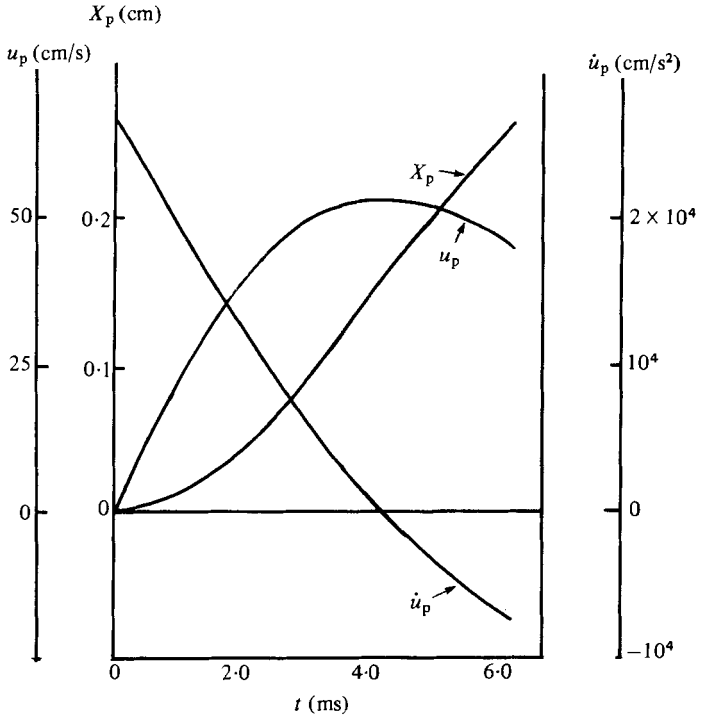

FIGURE 9. Typical variations of horizontal droplet displacement, velocity and acceleration in one test (numerical data for the test shown in the figure, no. 2514, are given in table 2).

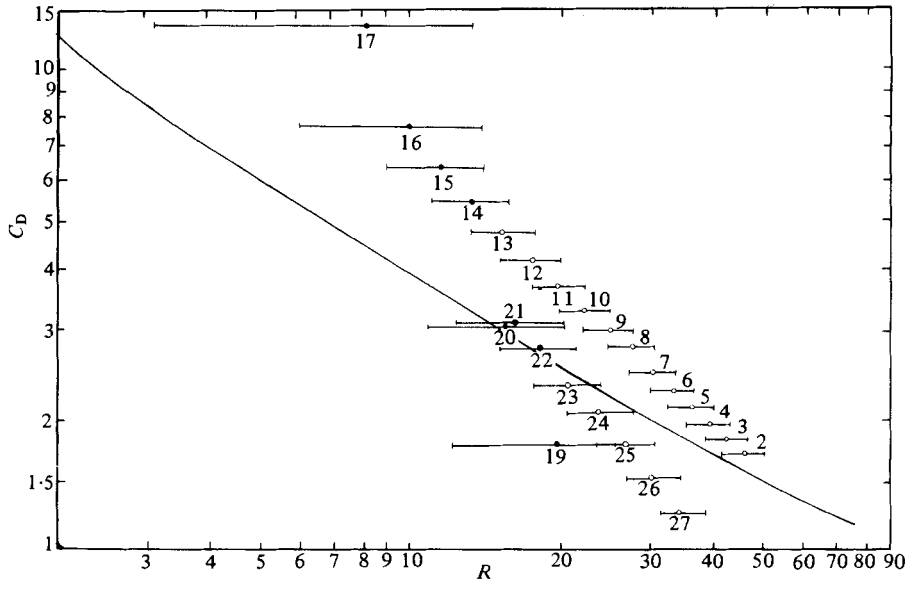

FIGURE 10. Drag-coefficient data for test no. 2514. The data for data-point no. 18, are $C_D = 127{\cdot}4$, $R = 2{\cdot}31$ (see table 2). Data denoted by filled symbols have estimated Reynolds-number errors larger than 15%.

Flash number	t (ms)	X_P (cm)	Y_P (cm)	u_t (cm/s)	A	R	C_D
1	0	0	0	448·5	—	48·41	—
2	0·250	0·0008	−0·0649	427·2	−6·2	46·11 ± 4·4	1·71 ± 0·32
3	0·500	0·0032	−0·1296	404·5	−7·2	42·77 ± 4·1	1·83 ± 0·35
4	0·750	0·0070	−0·1933	381·7	−8·1	39·54 ± 3·9	1·96 ± 0·38
5	1·000	0·0122	−0·2560	358·8	−9·2	36·42 ± 3·7	2·11 ± 0·41
6	1·250	0·0186	−0·3180	335·9	−10·6	33·41 ± 3·4	2·28 ± 0·45
7	1·500	0·0261	−0·3793	313·0	−12·2	30·50 ± 3·2	2·48 ± 0·51
8	1·750	0·0346	−0·4399	290·0	−14·3	27·70 ± 3·0	2·70 ± 0·56
9	2·000	0·0440	−0·4999	266·9	−16·8	25·01 ± 2·8	2·97 ± 0·64
10	2·250	0·0542	−0·5595	243·7	−20·0	22·43 ± 2·6	3·28 ± 0·73
11	2·500	0·0651	−0·6185	220·5	−24·0	19·97 ± 2·4	3·65 ± 0·86
12	2·750	0·0766	−0·6771	197·2	−28·9	17·64 ± 2·3	4·11 ± 1·03
13	3·000	0·0886	−0·7354	173·8	−34·9	15·46 ± 2·2	4·68 ± 1·28
14	3·250	0·1010	−0·7932	150·3	−42·0	13·46 ± 2·3	5·38 ± 1·75
15	3·500	0·1138	−0·8508	126·8	−50·0	11·65 ± 2·5	6·28 ± 3·24
16	3·750	0·1268	−0·9080	103·1	−63·1	10·02 ± 3·9	7·56 ± 6·63
17	4·000	0·1400	−0·9650	79·5	−132·7	8·24 ± 5·1	10·29 ± 10·45
18	4·250	0·1533	−1·0216	55·8	—	2·31 ± 1·2	127·45 ± 23·88
19	4·500	0·1667	−1·0780	32·1	−150·5	19·85 ± 7·5	1·77 ± 1·19
20	4·750	0·1800	−1·1340	8·3	−4·7	15·65 ± 4·7	3·05 ± 1·24
21	5·000	0·1932	−1·1897	−16·0	22·3	16·35 ± 3·9	3·09 ± 1·00
22	5·250	0·2063	−1·2451	−41·9	26·7	18·33 ± 3·1	2·75 ± 0·78
23	5·500	0·2191	−1·3001	−68·1	24·8	20·81 ± 3·1	2·39 ± 0·59
24	5·750	0·2316	−1·3547	−94·5	21·8	23·69 ± 3·1	2·06 ± 0·46
25	6·000	0·2439	−1·4088	−121·2	18·9	26·94 ± 3·4	1·77 ± 0·38
26	6·250	0·2557	−1·4624	−148·1	16·3	30·57 ± 3·7	1·53 ± 0·31
27	6·500	0·2671	−1·5155	−175·3	14·0	34·58 ± 3·9	1·31 ± 0·26

TABLE 2. Data from test no. 2514, $D = 135\ \mu$m

5. Conclusions

The data we have presented in this work, taken together with those presented earlier, show unequivocally that the drag coefficient for small spheres moving unsteadily in a fluid differs from the steady drag at the same Reynolds number. Further, the present work shows that the departures from the steady drag depend strongly on whether the relative fluid velocity increases or decreases in time.

Such trends cannot be explained in terms of existing theory. A plausible mechanism suggested to us by Professor G. K. Batchelor (1977, personal communication) on the basis of drag data having negative values of dU_r/dt was described recently by us (Temkin & Kim 1980). The proposed mechanism is the change of the recirculating region behind the sphere. Thus, we expect that, when $dU_r/dt < 0$, the deceleration of the free-stream velocity may result in a larger recirculating region, relative to the steady case, thereby producing a larger drag. Similarly, when $dU_r/dt > 0$, the acceleration of the free-stream velocity may be associated with a smaller recirculating region and, therefore, a smaller drag. The two distinct experimental trends presented in this work conform to the trends required by the above mechanism and, therefore, give support to it.

Other features of the results may also be described in terms of the same mechanism.

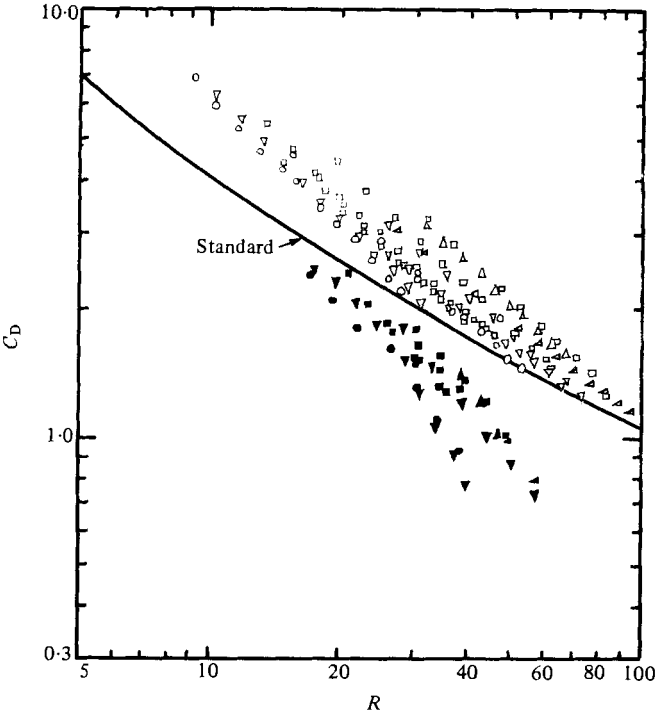

FIGURE 11. Drag-coefficient data. Open symbols, $dU_r/dt > 0$; filled symbols, $dU_r/dt < 0$. ○, ●, $D = 115\,\mu$m; ▽, ▼, 120 μm; □, ■, 135 μm; △, ▲, 152 μm; ◁, ◀, 167 μm.

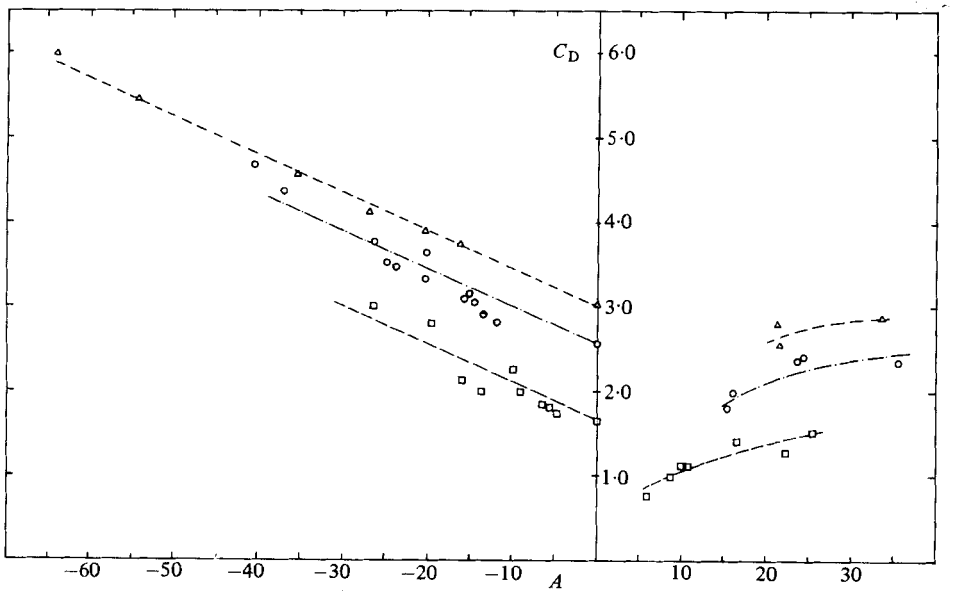

FIGURE 12. Variations of C_D versus A for several Reynolds numbers. △, $R \simeq 16$; ○, 21; □, 43.

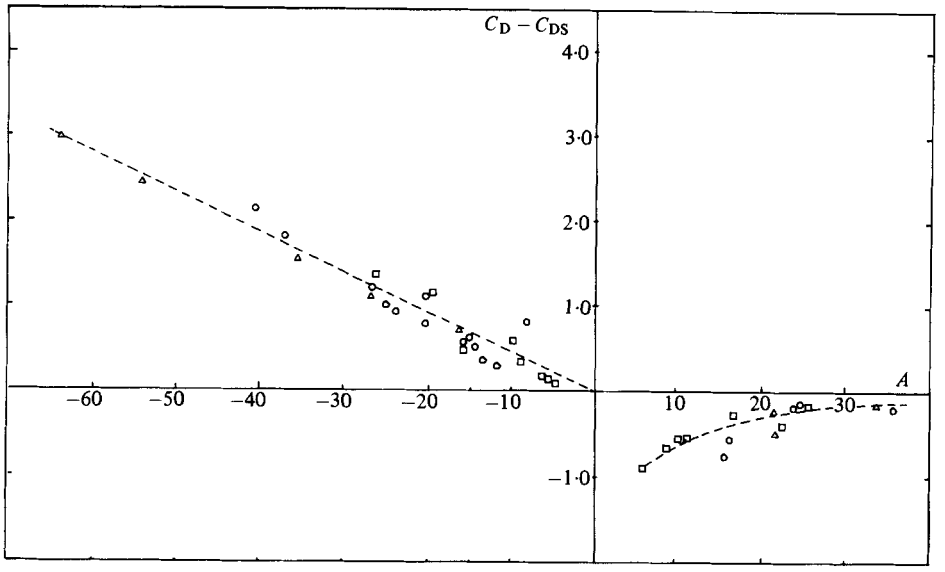

FIGURE 13. Difference between measured drag and steady drag as a function of A for the data shown in figure 12.

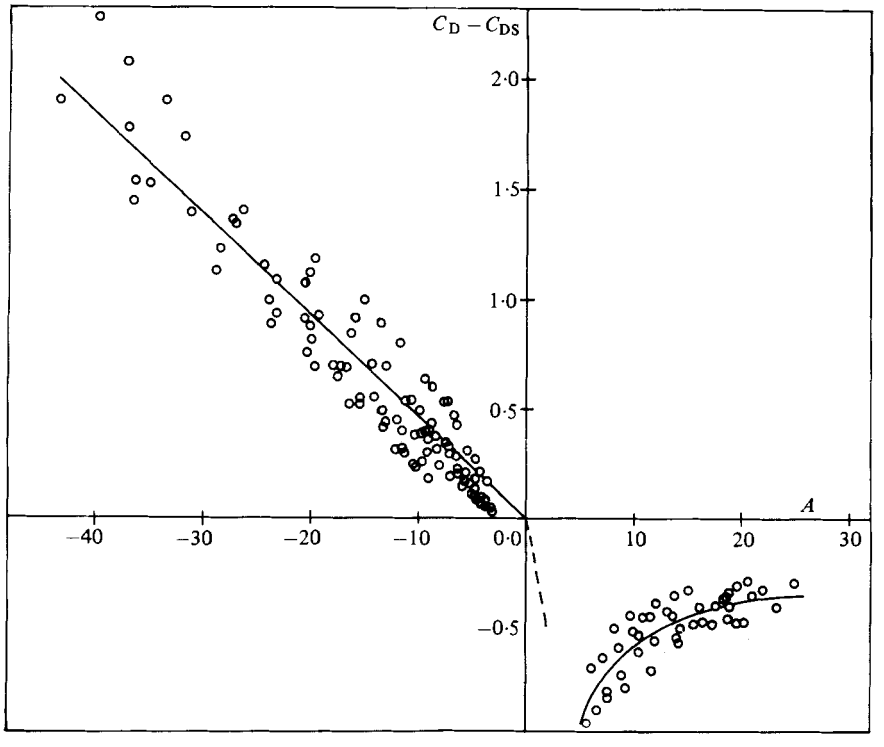

FIGURE 14. Difference between measured drag and steady drag as a function of the relative-acceleration parameter for all of the data having an estimated error in the Reynolds number smaller than 15%.

For example, as the magnitude of the relative deceleration increases, the departures from the steady drag increase, whereas for large positive relative accelerations the opposite effect seems to be true. The first trend seems to be compatible with the proposed mechanism because, as the deceleration increases, the size of the recirculating region also increases.

Consider now the opposite case. We know that, when $A = 0$, $C_D - C_{DS} = 0$, and that, when $A > 0$, the proposed mechanism predicts $C_D - C_{DS} < 0$. Suppose now that the relative acceleration is now increased from zero. Then we expect that the size of the recirculating region will decrease, resulting in a decrease of the drag relative to its steady value; that is $C_D - C_{DS}$ should become negative. As A increases further, $C_D - C_{DS}$ should become more negative. It is clear, however, that such a trend cannot continue indefinitely. One reason is simply that C_D cannot have negative values. Another is that, if the drag decreases as the recirculating region is reduced in size, the decrease is largely due to a change of the pressure drag. However, for smaller recirculating regions the contribution of the friction drag to the total drag is larger than that of the pressure drag, whereas for larger ones the trend is reversed. Thus, as that region is reduced, owing to an increase in A, a point will be reached where $C_D - C_{DS}$ will have a minimum, and beyond which $C_D - C_{DS}$ should increase with A.

While this argument is somewhat speculative, the observed data seem to support it, at least for $A > 5$, where $C_D - C_{DS}$ is observed to increase with A. Below $A = 5$, no direct support is presented because, as explained earlier, no data were obtained in the range $0 < A < 5$ that had estimated errors in the Reynolds number smaller than 15 %.† Nevertheless, it is clear that, for small values of A, $C_D - C_{DS}$ should approach zero from below, because, when $dU_r/dt = 0$, we must have $C_D = C_{DS}$. Thus, as $A \to 0$, the variations of $C_D - C_{DS}$ must be the type denoted by the dashed line in figure 14, as required by the proposed mechanism. (In fact, the dashed-line trend is followed by the $R \sim 21$ data that are available for $0 \leqslant A \leqslant 5$. Those data points are, however, not shown in figure 12 because their estimated errors in R are of the order of 25 %.)

Thus, based on the fact that the observed variations of $C_D - C_{DS}$ for positive and negative A seem to be consistent with those predicted by the proposed mechanism, we conclude that the departures from the steady drag that have been observed in our experiments are due to changes in the size of the recirculating region behind the sphere. An important corollary of this conclusion is that, for these unsteady flows, a recirculating region exists for Reynolds numbers as low as 9.

Finally, it should be added that drag coefficients obtained in one set of experiments may not be applicable to other situations unless they are of a similar nature. The motion reported here, and that reported earlier by Temkin & Kim are similar, at least in the forward part of the N-wave, where the droplets are accelerating. In fact, if we compare the drag coefficients obtained earlier in a uniform-cross-section shock tube with those presented here, it is possible to conclude that spheres accelerating in an impulsive type of flow with negative relative accelerations, experience a drag which is larger than the steady drag, and that the actual drag can be expressed by an equation of the form

$$C_D = C_{DS} - kA \quad (A < 0),$$

† For the case $A > 0$, we obtained a total of 115 data points having estimated errors smaller than 30 %. Of these, 86 had errors smaller than 20 % and only 47 points met the stringent 15 % limitation.

where k depends on the nature of the flow. On the other hand, the results for $A > 0$ presented here are the only ones available. It is, therefore, premature to extend their applicability to other unsteady situations.

This research was supported by the National Science Foundation under Grant NSF ENG 76–15045.

REFERENCES

CLIFT, R., GRACE, J. R. & WEBER, M. E. 1978 *Bubbles, Drops, and Particles*, chap. 11. Academic.

HILL, M. K. 1973 Behavior of spherical particles at low Reynolds numbers in a fluctuating translational flow. Ph.D. thesis, California Institute of Technology.

INGEBO, R. D. 1956 Drag coefficients for droplets and solid spheres in clouds accelerating in air streams. *N.A.C.A. Tech. Note* TN 3762.

KARANFILIAN, S. K. & KOTAS, T. J. 1978 Drag on a sphere in unsteady motion in a liquid at rest. *J. Fluid Mech.* **87**, 85–96.

KIM, S. S. 1977 An experimental study of droplet response to weak shock waves. Ph.D. thesis, Rutgers University.

LAMB, H. 1925 *The Dynamical Theory of Sound.* Dover.

LUNNON, R. G. 1926 Fluid resistance to moving spheres. *Proc. R. Soc. Lond.* A **110**, 302–326.

MEHTA, H. K. 1980 Droplet drag and breakup in shock-wave induced unsteady flows. Ph.D. thesis, Rutgers University.

ODAR, F. & HAMILTON, W. S. 1964 Forces on a sphere accelerating in a viscous fluid. *J. Fluid Mech.* **18**, 302–314.

REICHMAN, J. M. 1973 A study of the motion, deformation and breakup of accelerating water droplets. Ph.D. thesis, Rutgers University.

ROOS, F. W. & WILLMARTH, W. W. 1971 Some experimental results on sphere and disk drag. *A.I.A.A. J.* **9**, 285–291.

RUDINGER, G. 1974 Effective drag coefficients for gas-particle flow in shock tubes. *Trans. A.S.M.E.* D, *J. Basic Engng* **94**, 81–88.

SELBERG, B. P. & NICHOLLS, J. A. 1968 Drag coefficient of small spherical particles. *A.I.A.A. J.* **6**, 401–408.

TEMKIN, S. & KIM, S. S. 1980 Droplet motion induced by weak shock waves. *J. Fluid Mech.* **96**, 133–157.

TOROBIN, L. B. & GAUVIN, W. H. 1959 Fundamental aspects of solids–gas flows. III. Accelerated motion of a particle in a fluid. *Can. J. Chem. Engng* **37**, 224–236.